Quaternary Science Reviews 369 (2025) 109636

Contents lists available at ScienceDirect

Quaternary Science Reviews

journal homepage: www.elsevier.com/locate/quascirev

The topographic features and sedimentary environment potentially influenced the vegetation reconstruction in southwestern China since the MIS3

Xiao Zhang [a], Yuanfu Yue [b,*], Ziyan Zhang [a], Liuying He [b], Xinmeng Yuan [b], Xintian Yu [b], Qiuchi Wan [c], Cong Chen [d], Yongjie Tang [d], Zhuo Zheng [d], Kangyou Huang [d]

[a] College of Life Sciences, Zhejiang Normal University, 321004, Jinhua, China
[b] Guangxi Laboratory on the Study of Coral Reef in the South China Sea, Coral Reef Research Centre, School of Marine Sciences, Guangxi University, Nanning, 530004, China
[c] School of Geography, South China Normal University, Guangzhou, 510635, China
[d] Guangdong Key Lab of Geodynamics and Geohazards, School of Earth Sciences and Engineering, Sun Yat–sen University, Zhuhai, 519082, China

ARTICLE INFO

Handling Editor: Dr Yan Zhao

Keywords:
Pollen record
Southwestern China
Peat bog
MIS3
Biome reconstruction
Climate change

ABSTRACT

A series of pollen records from southwestern (SW) China has provided substantial evidence for the reconstruction of paleovegetation and paleoclimate in the region since the Last Glacial Period (LGP). However, studies investigating the relationship between paleoclimate and ecosystem changes during MIS3 remain limited, thereby constraining our understanding of the response of vegetation to climatic fluctuations on the glacial–interglacial timescale. Moreover, in comparison to local–scale topographic pollen sources, traditional lake sedimentary environments introduce a higher degree of uncertainty into vertical vegetation reconstructions. Here, we present a pollen record derived from a peat core of the Niangniang (NN) Mountain Wetland, aiming to reconstruct biome and climate variations over the past 37 ka. Our findings indicate that during the LGP, the study area was predominantly covered by deciduous broadleaved forests (DBLF), with *Quercus* (D) and other Betulaceae taxa as the main components. Although a sedimentary hiatus occurred in the core sediments between 18.5 and 4.6 ka, it is still possible to infer that from the LGP to the late Holocene, the forests surrounding the NN wetland transitioned from DBLF to evergreen broadleaved forests (EBLF), which were predominantly composed of *Castanopsis* and *Cyclobalanopsis*. Over the past 2400 years, the rapid expansion of associated plants, including Poaceae and *Pinus*, along with secondary taxa such as *Alnus*, has driven a gradual transition to the Alpine Shrubland and Meadow (ALSM) biome. This shift is largely attributed to early human activities and fires. By comparing these results with other pollen and climate records, we conclude that DBLF expanded extensively at medium–to–high altitudes during the LGP, rather than evergreen sclerophyllous *Quercus* forest (ESQF). Consequently, previous estimates of mean annual temperature (MAT) based on pollen data may have been inflated from the Last Glacial Maximum (LGM) to the Holocene. In addition to the drivers operating at the glacial–interglacial scale, the Atlantic Meridional Overturning Circulation (AMOC) plays a pivotal role in modulating the variability of the Indian Monsoon precipitation, which in turn influences biome succession in SW China.

1. Introduction

The mountain ranges and valleys in southwestern (SW) China have provided important glacial refuges (Boufford and van Dijk, 2004), and are global hotspots of biodiversity due to their extreme topographical features, together with intense climatic fluctuations associated with the Indian summer monsoon (ISM) and recurrent glaciations (Tang et al., 2015). In recent years, a series of pollen records have furnished essential data for the quantitative reconstruction of paleovegetation and paleoclimate in SW China, particularly since the Last Glacial Maximum (LGM). For instance, at higher altitudes, such as Tengchongqinghai (TCQH) (Zhang et al., 2020), Heqing (HQ) (Jiang et al., 2001), Caohai (CH) (Zhang et al., 2024) and Dianchi (DC) (Xiao et al., 2020), the high proportion of *Quercus* (ES) during the LGM implies a significant

* Corresponding author.
E-mail address: yuanfu.yue@gxu.edu.cn (Y. Yue).

https://doi.org/10.1016/j.quascirev.2025.109636
Received 4 April 2025; Received in revised form 23 September 2025; Accepted 25 September 2025
Available online 29 September 2025

southward expansion of evergreen sclerophyllous *Quercus* forests (ESQF) in this region. Simultaneously, other records indicate that deciduous broadleaved forests (DBLF), dominated by deciduous taxa like Betulaceae and *Quercus* (D), remained the dominant vegetation type in mid–to–high altitude mountains throughout the LGM (Deng et al., 2022; Li, K. et al., 2024). Moreover, studies on specialized taxa, such as *Pinus yunnanensis* (Pan et al., 2025), provide indirect evidence of small–scale vegetation evolution subsequent to the LGM. These studies on pollen records collected at different elevations in SW China have revealed distinct vegetation changes during the glacial–interglacial cycles (Shen and Xiao, 2018; Xiao et al., 2020) that have been closely linked to vertical biome shifts (Zhang et al., 2020). However, few investigated pollen records extend back through the Last Glacial Period (LGP, e.g., MIS3), and the low resolution of data acquired in previous works (Tang, 1992; Zhao et al., 2014; Zheng et al., 2016) has hindered precise spatial correlation and accurate dating of rapid climate changes during the LGP (Zhang et al., 2020).

Another critical issue that warrants attention is the limited focus in existing studies on the influence of topographic features and sedimentary environments on pollen–paleovegetation reconstruction. Pollen can be dispersed over distances ranging from dozens or even hundreds of km in flat terrain by wind and typically down to less than approximately 50 km in mountainous regions (Xu et al., 2016). Consequently, wind–dispersed pollen types with high productivity tend to be over–represented in pollen records. This over–representation leads to an overestimation of their proportion within vegetation types, such as *Pinus* (Wang et al., 2020). Most existing pollen records in SW China originate from lake sediments at various altitudes (Zhang et al., 2024). Larger lakes possess a robust ability to capture pollen transported by wind or water currents, thereby reflecting broader–scale mountain vegetation changes (Xu et al., 2016; Chevalier et al., 2020). In contrast, sedimentary environments with weaker pollen–trapping capabilities, such as wetlands, are more likely to accurately represent local vegetation succession characteristics (Deng et al., 2022). This divergence can result in significant differences in recorded vegetation types even among study sites in close proximity. For instance, during the LGP, the pollen record of TCQH lake in western SW China was predominantly characterized by ESQF. A significant portion of this pollen likely originates from the relatively high–altitude Gaoligong Mountain to the east (Xiao et al., 2015; Zhang et al., 2020). In contrast, merely 30 km to the north, Tengchongbeihai (TCBH) wetland was dominated by Coniferous and Mixed Forests (CLMX) during the same period (Zhang et al., 2019). Recent studies by Zeng et al. (2025) have utilized pollen analysis and ordination techniques to reconstruct the pollen dissemination characteristics of Gaoligong Mountain in SW China. Their findings indicate that the Asian summer monsoon, diurnally-varying orographic winds, and vegetation type characteristics all play roles in shaping pollen dispersal patterns in mountainous areas. Therefore, to achieve a more accurate reconstruction of the vegetation succession process in SW China since the LGP, it is essential to obtain additional pollen records from non–traditional lake sources.

Furthermore, the mechanisms driving biome changes in SW China since the LGP remain a subject of debate. Pollen records and simulation studies suggest that annual or monthly solar radiation may have been the primary factor influencing regional vegetation succession since the LGM (Xiao et al., 2015; Zhang et al., 2023). During the growing season, solar radiation plays a crucial role in influencing plant photosynthesis and growth, thereby determining the types and spatial distribution of vegetation over time. Other research has highlighted the significant impact of high–latitude ice volume on biome changes in the Yunnan–Guizhou Plateau (Zhang et al., 2024). High–latitude ice volume can significantly influence global sea level and atmospheric circulation patterns. These changes, in turn, have a profound impact on the climate of the Yunnan–Guizhou Plateau and contribute to local biome changes. Additionally, other factors such as surface temperature variations in the Indian Ocean–Western Pacific Warm Pool (a major driver of climate variability in the region; Xiao et al., 2014; Zhang et al., 2020), the north–south shifts of the Intertropical Convergence Zone (ITCZ) (Xiao et al., 2020), and fluctuations in the strength of the Atlantic Meridional Overturning Circulation (AMOC) (Zhang et al., 2024) have collectively exerted an influence on the characteristics of regional vegetation succession at various temporal scales. Thus, further research is necessary to elucidate the complex interactions of these influencing factors on biome change in SW China.

The Niangniang (NN) Mountain Wetland is situated in the western region of the Yunnan–Guizhou Plateau. The surrounding area features a karst peak cluster landform (Li, S.M. et al., 2024; Yue et al., 2024). Numerous cushion–shaped peat wetlands have developed and are distributed across the basaltic mountain plateau in this region. Our aim in this study is to reconstruct the biome succession in the eastern mountainous regions of the Tibetan Plateau and the Hengduan Mountains since MIS3. To achieve this, we present a pollen record retrieved from the NN subalpine wetland and quantitatively reconstruct local biome and climate variations since 37 ka. We systematically compare this pollen with numerous pollen and other paleoclimate records from SW China. Among these, especially noteworthy is the record of Caohai (CH) lake, which, despite its proximity, exhibits marked differences in sedimentary environments (Zhang et al., 2024). Through this comparison, we can reconstruct the biome succession in the target regions with greater precision and offer unique insights. This approach not only enhances the accuracy of quantitative climate reconstructions in the ISM region but also provides new perspectives on the mechanisms of related climate forcing.

2. Study area

2.1. Geographical setting

The NN Mountain is within the territory of the Yunnan–Guizhou Plateau, which is a transitional zone from the Tibetan Plateau to areas of lower altitude (Fig. 1). The wetland atop the NN Mountain (26°34′40″–26°36′38"N, 104°45′29″–104°48′45"E, 2050 m a.s.l.) represents one of the most well preserved plateau wetlands in SW China, renowned for its remarkable biodiversity (Zhou et al., 2022). The climate of the NN Mountain is mainly influenced by the ISM. The warm and moist air masses associated with the ISM lead to warm winters and hot summers. The study area has a subtropical humid monsoonal climate with around 78 % of its precipitation falling between May and October, when moist winds from the Arabian Sea and Bay of Bengal bring abundant rainfall. The mean annual temperature (MAT) of the study area is around 13.5 °C, while the mean annual precipitation (MAP) is approximately 1350 mm (Yue et al., 2024).

2.2. Modern vegetation

The current distribution of vegetation types in the NN Mountain and adjacent mountainous regions is closely correlated with the elevational gradients of the Tibetan Plateau. More specifically, the vegetation in the mountain ranges of SW China can be categorized into a series of distinct vegetation belts (Tang, 2015).

The lowest elevation belt, characterized by tropical rainforest (TRFO), occurs in Yunnan Province at the altitudes below 1000 m a.s.l. This ecosystem is predominantly composed of species from the families Fabaceae, Meliaceae, and Sapindaceae, with a minor presence of gymnosperms such as *Pinus*, Cycadaceae, and Podocarpaceae. Evergreen broadleaved forest (EBLF) typically develops between 1000 and 2400 m a.s.l, where it is primarily dominated by Fagaceae species including *Cyclobalanopsis delavayi*, *C. glaucoides*, and *Castanopsis delavayi*, alongside associated species like *Cinnamomum glanduliferum* and *Schima wallichii*. Coniferous forests, notably those dominated by *Pinus yunnanensis*, are prevalent in the upper elevations of this zone. Additionally, the lower boundary of this elevation belt exhibits some transitional

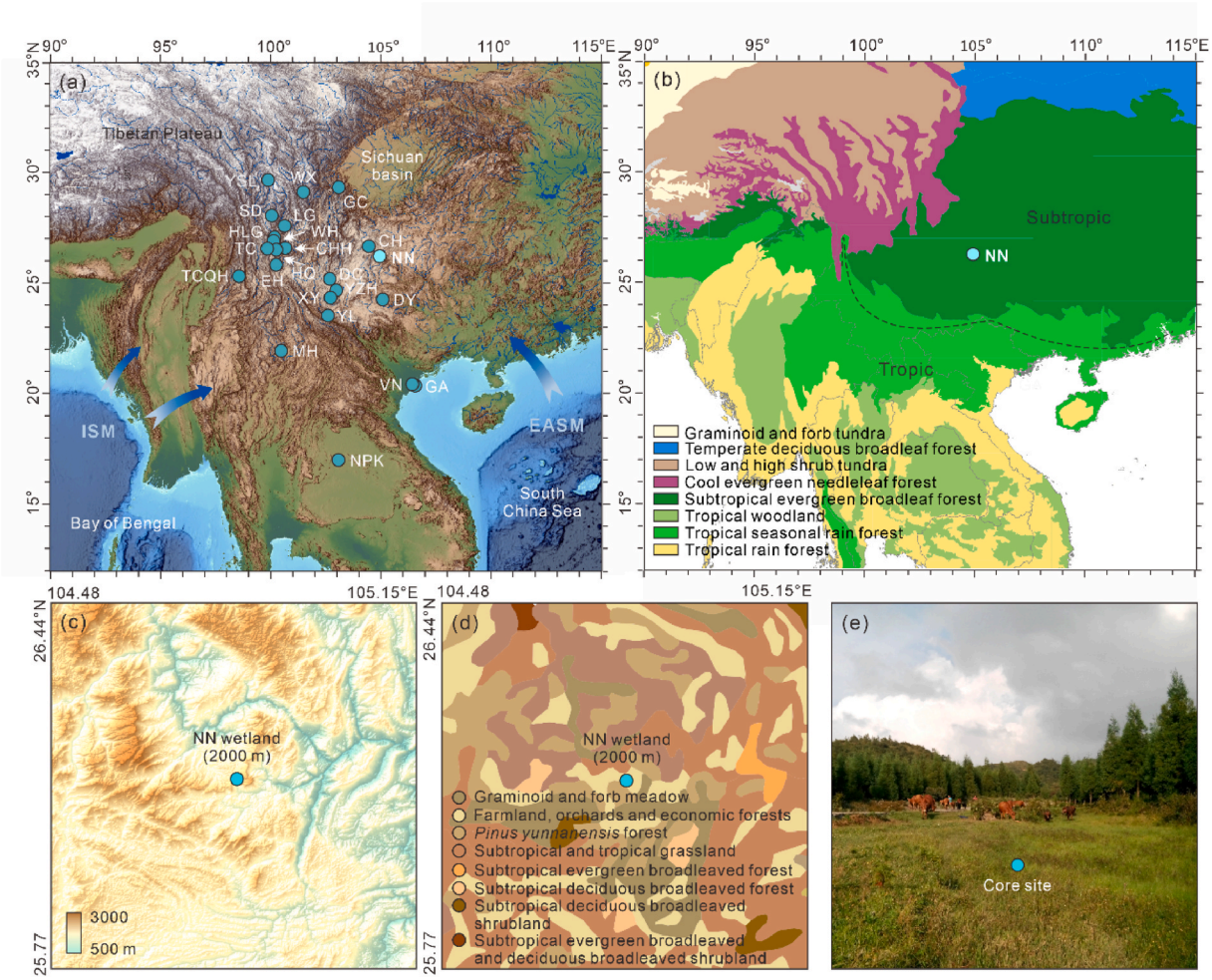

Fig. 1. (a) Topography and location of the NN wetland and the cores used for correlation. Dark green dots indicate the YSL profile (Shi et al., 2011), Wuxu (WX) (Zhang et al., 2016), Shudu (SD) (Cook et al., 2011, 2013; Yao et al., 2017), Haligu (HLG) (Song et al., 2012), Wenhai (WH) (Yao et al., 2015), Chenghai (CHH) (Xiao et al., 2017), Tiancai (TC) (Xiao et al., 2014), Lugu (LG) (Shen and Xiao, 2020), Tengchongqinghai (TCQH) (Xiao et al., 2015; Zhang et al., 2020), Dianchi (DC) (Xiao et al., 2020), Xingyun (XY) (Chen et al., 2014a, 2014b), Yangzhonghai (YZH) (Wang et al., 2020), Yilong (YL) (Li, K. et al., 2024) and Menghai (MH) lake (Tang, 1992); Ganchi (GC) wetland (Deng et al., 2022); Heqing (HQ) basin (Jiang et al., 2001; Xiao et al., 2007); Dayin (DY) cave (Zhang et al., 2024), VN/GA (Li et al., 2009), NPK (Penny, 2001); (b) Vegetation map of SW China (Zhang, 2007). (c) local topography and location of the NN wetland. (d) local vegetation around NN wetland (Zhang, 2007). (e) The surrounding environment of the core site. (For interpretation of the references to color in this figure legend, the reader is referred to the Web version of this article.)

forest types that incorporate elements of the tropical flora found at lower altitudes. From 2400 to 2700 m a.s.l., the vegetation types give way to conifers and deciduous broadleaved trees dominated by *Juniperus formosana*, *Pinus yunnanensis*, *Quercus fabri*, *Q. aliena*, *Corylus yunnanensis*, *Populus yunnanensis*, *Salix cavaleriei*, and *Alnus mengtze*. The dominant forest types here are deciduous broadleaved forest (DBLF) and mixed broadleaved forest (EBLF/DBLF). Between 2400 and 2700 m a.s.l, the vegetation transitions to DBLF, with dominant species including *Juniperus formosana*, *Pinus yunnanensis*, *Quercus fabri*, *Q. aliena*, *Corylus yunnanensis*, *Populus yunnanensis*, *Salix cavaleriei*, and *Alnus mengtze*. Additionally, evergreen sclerophyll *Quercus* forest (ESQF) dominated by sclerophyll *Quercus* species is common and/or dominant in a belt centered between 2500 and 3600 m in the southeastern parts of the Tibetan Plateau and SW China (Yang et al., 2009). Cold mixed forest (CLMX), primarily composed of cold–tolerant conifers such as *Abies*, *Picea*, and *Pinus*, is predominantly distributed between elevations of 3300 and 4200 m a.s.l. As elevation continues to increase, alpine shrubland, meadow, and tundra (ALSM) ecosystems are prevalent, characterized by dominant species from the Cyperaceae, Poaceae, and Ranunculaceae. The permanent ice belt generally forms at elevations above 4800–5000 m. The zonal vegetation of the NN Mountain primarily consists of EBLF, secondary forests, and certain cash crops, such as *Toxicodendron vernicifluum* and *Camellia oleifera* (Fig. 1d).

3. Materials and methods

3.1. Materials

The NN core was taken from the alpine wetland of the NN Mountain in the western Guizhou Province (Fig. 1e). The research site is not influenced by any rivers in its vicinity. The core is 150 cm long and covers all the sediment to the bedrock.

3.2. Methods

3.2.1. Laboratory analysis

The samples were collected at 1 cm intervals at the top 50 cm of the core and at 0.5 cm intervals towards the bottom (50–150 cm). In total, a collection of 245 samples was obtained. So, for each pollen sample, about 1 g of sediment was weighed and processed by heavy liquid separation (Moore et al., 1991; Yue et al., 2012). On average, 510 terrestrial pollen grains were counted per individual sample. Based on

the above counting method, all percentages quoted for pollen grains (from conifers, arboreal and non–arboreal taxa) in this work are based on the summed counts of pollen grains from terrestrial taxa. We used previously established morphological criteria to divide the complex *Quercus* pollen in SW China (Zhang et al., 2018). TILIA 3.0.1 (Grimm, 1991–1993) was used to calculate pollen percentages and plot the pollen diagram.

3.2.2. Biomization reconstruction

Vegetation reconstruction was conducted using the biomization technique based on previously reported plant functional types (PFTs) (Ni et al., 2014; Zheng et al., 2023), specifically employing the biome classifications derived from the pollen record of Caohai (CH) lake (~100 km southeast from NN site) (Zhang et al., 2024). Consistent with the CH lake records, all pollen taxa identified from the NN core were assigned to 17 PFTs and subsequently aggregated into 6 biomes relevant to the study area. When this biome reconstruction method was applied to modern pollen spectra for validation, the majority of samples were accurately classified according to previous studies (Zhang et al., 2024).

3.2.3. Statistical analysis

To simplify the analysis of the relationships between the ecological properties of the different pollen taxa and climatic variables, and to establish a quantitative framework for linking vegetation dynamics to paleoclimatic changes, we performed a principal component analysis (PCA) on the pollen dataset (Birks et al., 1998). Statistical analyses were based on the abundances (expressed as percentages) of pollen taxa detected in at least five samples with relative abundances exceeding 2 %; 30 pollen taxa satisfied these requirements. The gradient length was below 2 (1.32 in this study) standard deviation (SD) units, so the PCA method was considered appropriate for analyzing pollen assemblages with respect to interspecific correlations using square root transformation of pollen percentages. Statistical analyses were performed using Canoco 5.0 (Braak and Smilauer, 2002), with results visualized through biplot projections that simultaneously display taxon compositions and sample groupings. This integrative approach enabled us to identify dominant vegetation patterns and their climatic drivers across the studied stratigraphic interval.

4. Results

4.1. Sediment lithology and core chronology

Based on the color and lithological characteristics of the core sediments in the field, the 150 cm long NN sediment can be roughly divided into 5 layers from bottom to top (Fig. 2). The sediment from 150 to 126 cm consists of gray clay interbedded with wood fragments (140–136 cm) and plant remains. This is followed by a layer of dark peat with higher organic content (126–100 cm), which is identical to that observed between 80 and 50 cm. The deposits between 100 and 80 cm consist of silty dark gray clay and the uppermost 50 cm of the NN core mainly consists of silty gray clay.

The core's chronology was determined through accelerator mass spectrometry (AMS ^{14}C) dating of nine plant fragments and bulk sediment samples, which were analyzed at the Xi'an Accelerator Mass Spectrometry Center and Beta Analytic Inc. (Miami, USA) (Table 1). Given the study area's dominance of Carboniferous-Permian limestone, sandstone, and minor coal layers, the ^{14}C dating results from sediment samples collected at the NN wetland may be affected by the hard-water effect typical of karst sedimentary environment (Kong et al., 2010). This effect occurs when initial ^{14}C radioactivity in aquatic sediments is lower than contemporary atmospheric levels, causing apparent age overestimation of organic materials—an effect more pronounced in lake sediments. Notably, because the core was retrieved from an alpine wetland, the likelihood of hard-water effect influence is low. The age-depth model was established using the Bayesian Bacon method

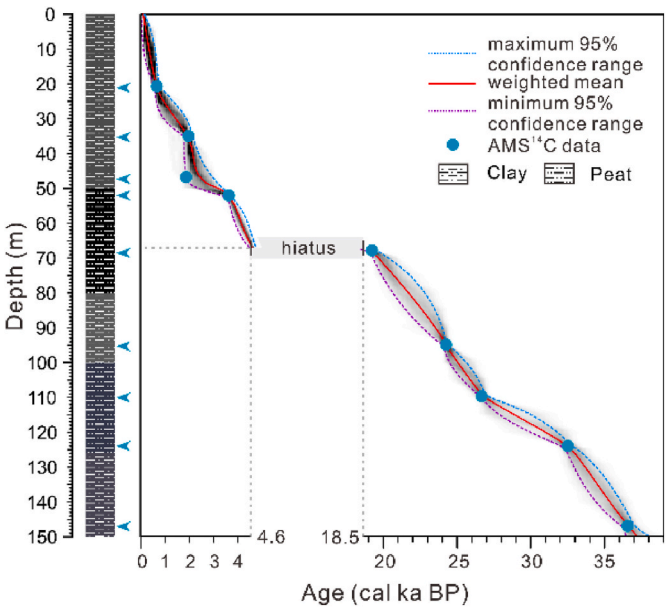

Fig. 2. Lithology and age/depth model of the NN core.

(Blaauw and Christen, 2011). It indicates that, due to the presence of a sedimentary hiatus, the core can be clearly divided into two distinct sections at a depth of 67 cm. The lower section spans from 150 to 67 cm, corresponding to an age range of 37.2 to 18.5 ka, while the upper section extends from 67 cm to the surface (0 cm) with an age range of 4.6 ka to the present (Fig. 2). The average temporal sampling resolutions of the two components are approximately 56 years and 114 years, respectively.

4.2. Fossil pollen and charcoal record

A total of 93 pollen and spore types were identified in 245 samples retrieved from the NN core. The most abundant and representative taxa are shown in the pollen diagram (Fig. 3). In samples from the glacial interval, the pollen assemblages are dominated by arboreal and herbaceous pollen. The most abundant taxa are *Quercus* (D), Betulaceae (*Corylus*, *Betula*, *Carpinus*) and Poaceae, which collectively account for 70–85 % of the total pollen content. These taxa are typical of a relatively cold and dry climate, which was characteristic of the glacial interval. Conversely, the dominant pollen taxa in assemblages from the Holocene are *Cyclobalanopsis* and *Castanopsis* followed by *Pinus*; other frequently detected taxa include arboreal taxa such as *Tsuga*, *Alnus*, *Eurya* and herbaceous taxa such as *Artemisia*, Asteraceae and Lamiaceae. To better understand the temporal variation of pollen assemblages, a Constrained Incremental Sum of Squares (CONISS) analysis was performed on the pollen data. Based on a CONISS analysis of the pollen data, the pollen sequence was divided into the following five main zones.

Zone 1 (37.2–27.4 cal ka BP, 150–112 cm)

In this zone, the mean percentage of arboreal pollen reaches a notably high value of 67.9 %, with *Quercus* (D) serving as the dominant taxon, accounting for an average of 24.9 %. Other common arboreal taxa include *Corylus* (6.9 %), *Carpinus* (5.1 %), *Betula* (3.2 %), and *Fagus* (3.3 %). Among non–arboreal pollen, Poaceae has the highest proportion at 18.7 %. This zone is further subdivided into two subzones, namely ***Zone 1a*** *(37.2–32.5* cal *ka BP, 150–*127 cm*)* and ***Zone 1b*** *(32.5–27.4* cal *ka BP, 127–*112 cm*)*. Compared to Zone 1a, the proportion of *Quercus* (D) in Zone 1b increased from 20.1 % to 29.1 %. Additionally, there were slight increases in other deciduous taxa such as *Betula* (from 2.5 % to 3.8 %), *Carpinus* (from 4.5 % to 5.5 %), and *Fagus* (from 2.9 % to 3.6 %), while the proportion of coniferous taxa decreased (from 9.1 % to 6.4 %). The composition of non–arboreal/herbaceous pollen remained largely

Table 1
AMS radiocarbon dates of samples from the NN core.

Depth (cm)	Lab code	Materials	^{14}C date (a BP)	Error (±a)	Calibrated age (cal a BP, 2σ)	Mid–point (cal a BP)
21	Beta 503983	Dark clay	480	30	496–542	518
35	Beta 503984	Dark clay	1880	30	1714–1840	1785
47	Xi'an 01	Dark clay	1617	28	1411–1538	1479
51.5	Beta 503985	Dark clay	3220	30	3375–3471	3426
68	Xi'an 02	Dark clay	15801	56	18909–19191	19054
95	Xi'an 03	Dark clay	20072	62	23879–24249	24071
110	Beta 506744	Dark clay	22240	80	26298–26936	26599
124	Xi'an 04	Dark clay	28250	120	31855–32934	32312
147	Beta 360342	Gray dark clay	32050	220	36000–36924	36391

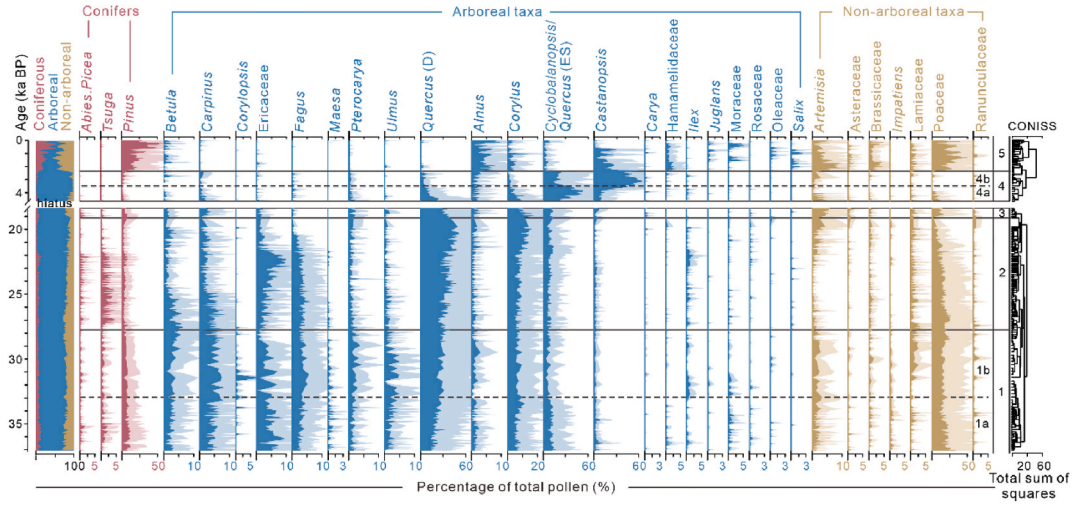

Fig. 3. Pollen percentage diagram of selected taxa in the NN core. There was a sedimentary hiatus between 4.6 and 18.5 ka. The solid and faded plots show the same percentage values on different scales.

unchanged.

Zone 2 (27.4–19.1 cal ka BP, 112–69 cm)

Compared to the preceding zone, Zone 2 exhibits an increased proportion of arboreal pollen (75.9 %), while the proportions of coniferous and non–arboreal pollen have both decreased to some extent. Notably, this zone is characterized by a significant rise in *Quercus* (D) to its highest percentage (36.9 %). Additionally, the proportion of *Corylus* has increased to 8.7 %. However, the proportions of other deciduous taxa that were relatively high in Zone 1 have slightly decreased, such as *Betula* (2.3 %), *Carpinus* (3.0 %) and *Fagus* (2.9 %). Among conifers, the most pronounced change is observed in *Tsuga*, which has increased from 0.7 % to 1.8 %. In terms of non–arboreal/herbaceous pollen, the proportion of Poaceae has decreased to 15.2 %, and *Artemisia* has also declined from 1.7 % to 1.0 %, with minimal changes in other herbaceous taxa.

Zone 3 (19.1–18.5 cal ka BP, 69–66 cm)

The variations in the proportions of conifer, arboreal, and non–arboreal pollen within Zone 3 were relatively minor. However, significant changes were observed among certain deciduous and evergreen taxa. Specifically, the proportions of *Quercus* (D) (27.7 %) and *Fagus* (0.3 %) exhibited a significant decline. Additionally, there was a slight decrease in *Betula* (1.1 %) and *Carpinus* (2.3 %). Conversely, the primary evergreen taxa, *Castanopsis* and *Cyclobalanopsis*, increased to 6.5 % and 18.4 %, respectively. Among non–arboreal pollen, *Artemisia* reached its highest proportion in the entire pollen diagram at 4.3 %, while Poaceae showed a slight reduction to 12.1 %.

Zone 4 (4.6–2.4 cal ka BP, 66–51 cm)

Zone 4 commenced at 4.6 ka due to the influence of the sedimentary hiatus. This zone is characterized by a markedly elevated arboreal pollen content (92.2 %), primarily dominated by *Cyclobalanopsis* (36.5 %) and *Castanopsis* (30.6 %). The proportions of coniferous and non–arboreal pollen both exhibit significant reductions. This zone can be further subdivided into two subzones:

Zone 4a (4.6–3.7 cal ka BP, 65–57 cm)

This zone exhibits the highest concentration of *Cyclobalanopsis* pollen (44.9 %) throughout the entire core. Additionally, several other evergreen taxa showed an increase, including *Ilex* (0.6 %). Conversely, the proportions of *Quercus* (D) and *Corylus* pollen declined significantly to 12.9 % and 5.6 %, respectively. The percentage of Poaceae within the non–arboreal pollen fraction also decreased from 12.1 % to 4.9 %.

Zone 4b (3.7–2.4 cal ka BP, 57–51 cm)

Compared to Zone 4a, the arboreal pollen content in Zone 4b is significantly higher at 94.5 %, while the proportions of coniferous and non–arboreal pollen are markedly lower at 1.8 % and 3.6 %, respectively. The most distinctive feature of this zone is the rapid increase in the proportion of *Castanopsis* pollen, which reaches its peak at 47.8 %, whereas the proportion of *Cyclobalanopsis* pollen declines to 28.1 %.

Zone 5 (since 2.4 cal ka BP, 51–0 cm)

In this zone, the proportion of arboreal pollen experienced a rapid decline to its lowest recorded level of 38.6 %, while both coniferous (27.1 %) and non–arboreal pollen (34.3 %) reached their highest levels. The increase in coniferous pollen was primarily attributed to a substantial rise in *Pinus* from 1.9 % to 26.9 %. The elevation in non–arboreal pollen was driven by significant increases in Poaceae, *Artemisia*, and Brassicaceae, with Poaceae notably rising to 25.8 %. Additionally, secondary taxa such as *Alnus* (5.6 %) and *Salix* (0.34 %) also exhibited marked upward trends.

4.3. Statistical analysis

PCA was conducted on the relative pollen frequencies to identify the key climatic factors influencing vegetation dynamics. The analysis of

245 NN core samples, encompassing 30 taxa, resulted in the first and second principal components (PCs), with their eigenvalues accounting for 51.3 % and 37.6 % of the total variance, respectively (Fig. 4). Taxa with positive loadings on PC1 primarily comprise common tropical and subtropical evergreen broadleaved forest species such as *Castanopsis* and *Cyclobalanopsis*. These evergreen species typically thrive in warmer climates. Conversely, taxa with negative loadings on PC1 predominantly include cold–tolerant deciduous trees like *Quercus* (D), *Fagus*, *Betula*, Ericaceae, and *Corylus*, as well as temperate conifers such as *Abies/Picea* and *Tsuga* (Fig. 4a). The presence of these cold–tolerant taxa in the negative loading group indicates that PC1 predominantly captures the influence of temperature on pollen taxa. Taxa with positive loadings for PC2 are primarily herbaceous taxa, including Poaceae, *Artemisia*, and certain deciduous taxa, whereas evergreen taxa such as *Castanopsis*, *Cyclobalanopsis*, and *Ilex* exhibit negative loadings. This suggests that PC2 may primarily reflect moisture conditions at the site, where positive values correspond to drier conditions and negative values indicate wetter conditions (Fig. 4a). Based on these interpretations of PC1 and PC2, Zone 2 is likely characterized by the driest or coldest conditions, while Zone 4a may represent the warmest or wettest environment (Fig. 4b).

To further explore the relationship between vegetation distribution and climate conditions over the past 21 ka in SW China, we compared the PC1 and PC2 curves with the TraCE–simulated MAT and MAP (Liu et al., 2009). By making this comparison, we aimed to validate whether the principal components obtained from the PCA could serve as reliable proxies for temperature and precipitation. Although a sedimentary hiatus exists between 18.5 and 4.6 ka, the trends identified in the PCA results align closely with those of the simulated reconstructions, indicating that the principal components may function as proxies for temperature (PC1) and precipitation (PC2), as suggested by earlier studies. (Fig. 4c). This finding implies that vertical biome shifts were predominantly influenced by temperature variations along elevation gradients and changes in monsoon precipitation intensity (Xiao et al., 2020; Zhang et al., 2024).

4.4. Biome reconstructions

Biome reconstructions play a crucial role in understanding the long–term ecological dynamics in SW China (Ni et al., 2014). In previous research, we effectively reconstructed the current biomes of SW China using modern pollen samples. The findings indicated that the shifts in pollen–based biomes were largely consistent with the vertical vegetation changes observed in the eastern mountains of the Tibetan Plateau (Zhang et al., 2024). As illustrated in Fig. 5, this study employed the same biome reconstruction method for the NN core. Biome scores indicated that during the LGP, the dominant biome was consistently

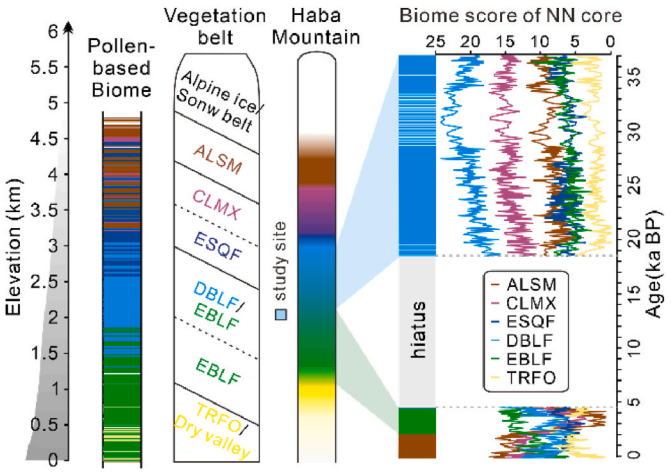

Fig. 5. Compare the pollen–based Biome in SW China (left) (Zhang et al., 2024), the modern mountainous vegetation types (middle) and the biome variations of the NN core (right). The elevated ALSM biome score observed between 2.4 and 0 ka are likely attributable to agricultural activities rather than natural factors.

DBLF (zones 1–3), especially prominent during MIS3, when the score peaked. During this time, CLMX and ALSM also showed relatively high biome scores, while the scores for EBLF and TRFO were the lowest. During the late Holocene (Zone 4), the biome score of EBLF reached its peak, indicating a significant shift in vegetation types during the transition from the LGP to the Holocene. Although the exact timing of the transition from DBLF to EBLF remains uncertain, a comparison with the biome reconstruction results from the adjacent CH core suggests that it likely occurred during the late deglaciation period or the early Holocene (Zhang et al., 2024). After 2.4 ka, ALSM emerged as the biome with the highest score, coinciding with a marked increase in *Pinus* and Poaceae pollen abundance (zone 5), which may be closely associated with human activities such as large–scale deforestation for agriculture and expansion of pastoral areas.

5. Discussion

5.1. Biome variations of NN and CH record

The most abundant pollen taxon in the NN fossil record from the LGP is *Quercus* (D), accompanied by other deciduous trees such as *Betula*, *Carpinus*, *Fagus*, Ericaceae (e.g., *Rhododendron*), and *Ulmus*. The biome result also indicates that the DBLF score has consistently been the highest, particularly during the MIS3 (Fig. 6). In modern East Asia, DBLF

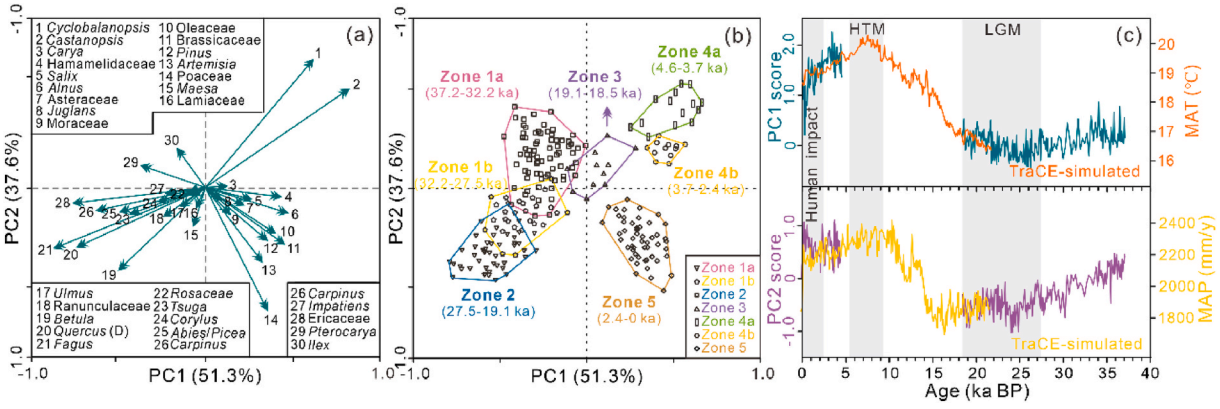

Fig. 4. PCA ordination of pollen percentage data. (a) PCA results based on selected pollen taxa. (b) Biplot of the PCA result for pollen data; (c) Comparison of PC1 (PC2) values and the local temperature (precipitation) simulated using TraCE21 (Liu et al., 2009).

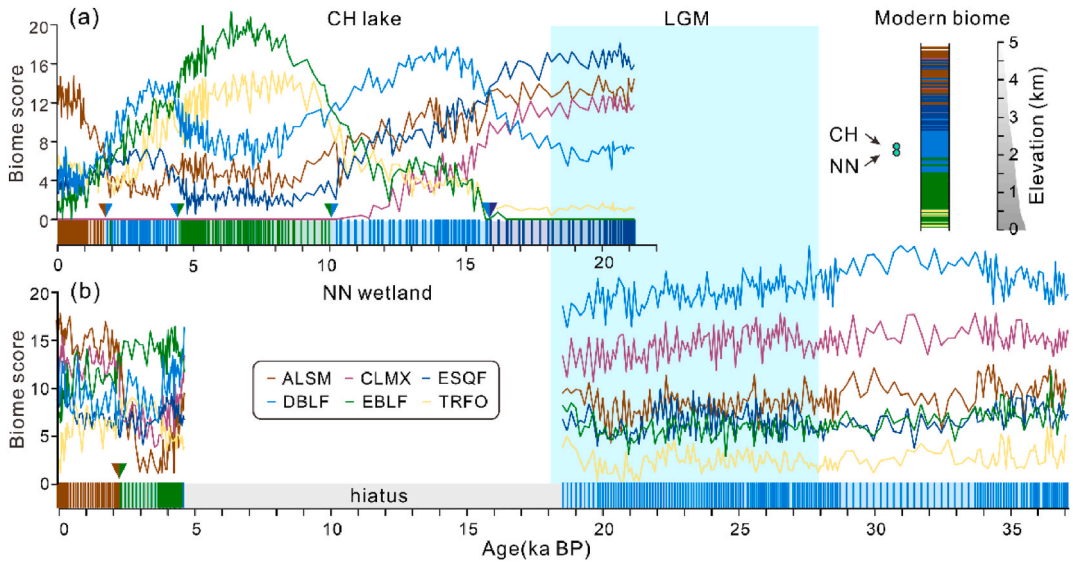

Fig. 6. Compare the biome scores recorded by (a) CH (Zhang et al., 2024) and (b) NN cores. The modern biomes found at different altitudes in SW China are also shown on the upper right side (Zhang et al., 2024). As illustrated in Fig. 5, the elevated biome scores of ALSM since 2.4 ka are closely associated with human activities.

is predominantly distributed north of 32° latitude, while in southwestern regions, only scattered patches of DBLF exist, likely due to the influence of the winter climate in this area (Tang, 2015). Although DBLF can be found within an elevation range of 300–3000 m a.s.l. (Flora of China Editorial Committee, 2013), they typically dominate at altitudes between 2000 and 2500 m a.s.l. (Zhou, 1981). This suggests that the vegetation types during the LGP exhibited a notable downward shift in altitude compared to contemporary vegetation (Tang, 2015).

To further understand the regional vegetation dynamics during the LGP, we compared the NN record with that of the CH core. The linear distance between the NN and CH cores is less than 100 km, and the sampling altitude difference is minimal (less than 200 m). Based on these geographical similarities, the vegetation types in the vicinity of these two records since the LGP were likely to have been relatively consistent. Wang et al. (2019) analyzed 14 pollen records from southern China and concluded that most of SW China was predominantly covered by temperate mixed coniferous and broadleaved forests or warm–temperate deciduous broadleaved forests during the LGP. While this general pattern provides a regional context, the records from the NN and CH show some unique characteristics. During this period, particularly at the LGM, the biome differences recorded by NN and CH were notably distinct (Fig. 6), highlighting the local–scale variability in vegetation responses to the glacial climate. Before 16 ka, the biome score of CH consistently indicated a dominance of *Quercus* (ES), while DBLF exhibited a significant prevalence around NN during this interval. *Quercus* (ES) species are commonly encountered and often dominate in an altitudinal belt centered between 2500 and 3600 m a.s.l. in the southeastern Tibetan Plateau and SW China (Yang et al., 2009). This elevation range is significantly higher, by approximately 500–800 m, than that of deciduous DBLF currently distributed in the southwestern region (Tang, 2015). *Quercus* (ES) exhibits notable adaptability to very cold and arid climates as well as nutrient–deficient soils. These conditions typically limit the growth of most deciduous broadleaved trees such as *Alnus*, *Betula*, and *Carpinus*, and other deciduous or evergreen Fagaceae members like *Quercus* (D) and *Cyclobalanopsis*, which are predominantly found at lower elevations (Zhou et al., 2007). Given the distinctive ecological characteristics of *Quercus* (ES) and its specific elevation range, it is plausible that these factors contributed to the notably lower vertical distribution of vegetation types recorded by the NN core compared to those documented in the CH record during the LGM.

We posit that the variation in pollen sources across different sites and the differing capacities of sedimentary environments to retain pollen are likely the primary factors contributing to this discrepancy. Firstly, CH is a typical karst lake formed under geological structural influences, with a catchment area of 380 km^2. It is surrounded by relatively high mountains, i.e. Xiliang (West, 2854 m), Yangjiao (East, 2519 m), Dalongcao (North, 2490 m) and Yingpan (South, 2360 m). Typically, pollen transport distances vary significantly depending on the terrain. For instance, in relatively flat terrains, pollen can be transported over distances ranging from dozens or even hundreds of kilometers, whereas in mountainous regions with dense vegetation, this distance is notably reduced to less than ~50 km (Xu et al., 2014). During summer, the ISM and associated precipitation transport pollen from the higher elevations of Xiliang Mountain on the western side to the CH water body, while during winter, the monsoon carries more pollen originating from Yangjiao Mountain on the eastern side. Unlike the CH core, the NN pollen sediments originated from the alpine wetland of NN Mountain. Within the pollen dissemination range, no other mountains with comparable or higher altitudes were present. Consequently, the pollen in the NN wetland primarily originated from a relatively localized area, which may lead to a more accurate representation of the local vegetation at that time but also limits the scope of regional vegetation information compared to the CH record. Thus, it is deduced that the high biome scores of ESQF and ALSM recorded by CH during the LGM do not straightforwardly imply that these high–altitude vegetation belts as a whole vertically descended by more than 1000 m (Zhang et al., 2024). This is because the composition of pollen records can be significantly affected by factors such as pollen sources and sedimentary environments. When calculated according to the altitude of the surrounding mountains of the CH core, the ESQF during this period is likely to have been concentrated within an altitude range of approximately 2300–2600 m. This indicates a downward shift of only about 500–800 m in comparison with the current situation (Fig. 7). Therefore, the area around CH may have been in the transition zone between DBLF and ESQF, while the area around NN was likely closer to the upper boundary of the DBLF belt during this period. Understanding these regional differences is crucial for comprehensively interpreting the vegetation evolution in this area, as it helps to identify the specific ecological niches and environmental gradients that influenced the distribution of different vegetation types. In previous studies, utilizing quantitative climate reconstruction results and the habitat characteristics of *Quercus* (ES), it

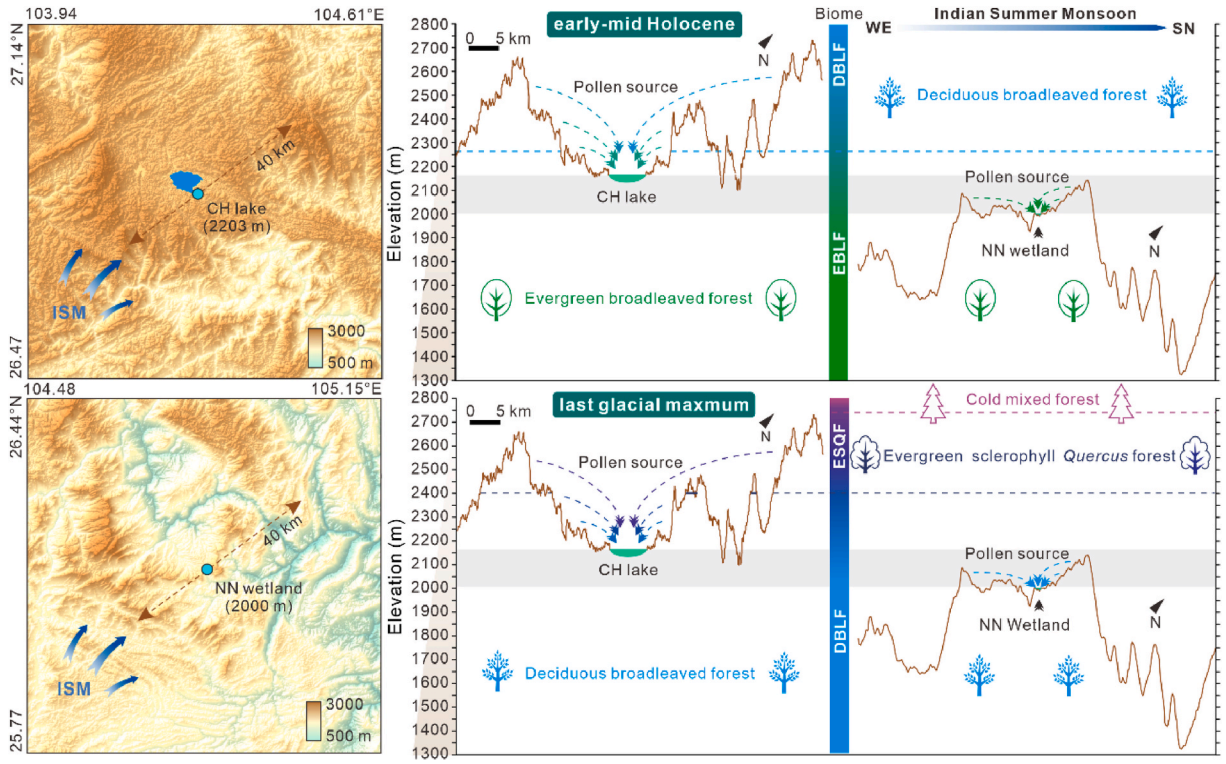

Fig. 7. The pollen sources of CH lake and NN wetland and the biome types of the mountain profiles during the early–mid Holocene and LGM.

was hypothesized that the biome transformation during the Heinrich event 1 (H1) period, as indicated by CH pollen records, could be closely associated with temperature fluctuations (Zhang et al., 2024). However, this conclusion may have underestimated the substantial influence of pollen sources. To gain a more accurate understanding of the biome transformation, it is essential to comprehensively consider factors such as pollen sources, sedimentary environments, and their interactions with climate change, in order to better reconstruct the historical vegetation dynamics in this area.

Since the deglaciation, with the gradual warming and increased humidity of the climate, the vertical vegetation zones in SW China have experienced an upward shift (Xiao et al., 2020). During this period, the CH sediment record clearly documented a transition in the surrounding mountain vegetation from DBLF to EBLF, which has been attributed to the intensification of the ISM (Zhang et al., 2024). Consistent with the CH records, the vegetation around NN also shifted from DBLF to EBLF between the LGP and the Holocene. Although sedimentary discontinuities prevent precise determination of the timing of this vegetation shift around NN site, evidence confirms that the EBLF boundary migrated upward by at least 300–500 m during the Holocene (Fig. 7). In the late Holocene (ca. 4–2 ka), the biome type in CH reverted from EBLF to DBLF, while regional vegetation type of NN wetland is EBLF, suggesting a slight downward migration of the alpine vegetation belt. The transition zone between EBLF and DBLF may be situated between 2000 and 2200 m during this period. Notably, since 2 ka, both CH and NN have recorded a clear shift to ALSM biome scores. We propose that the unusually high proportions of ALSM and DBLF during this period are attributable to elevated levels of Poaceae pollen (associated with ALSM) and *Alnus* pollen (linked to DBLF), likely resulting from human activities and fires. This also indirectly suggests that the anthropogenic disturbance in this area has been relatively consistent since around 2 ka.

5.2. Reassess the vegetation succession since the MIS3

To further elucidate the process in SW China since the MIS3, it is essential to understand the influence of topographic features and sedimentary environments on pollen records. Consequently, we systematically categorized previous pollen data, including those from NN, into four distinct types of study sites (Table 2).

1. The pollen source area is extensive, typically exceeding 30–50 km, with surrounding mountains of higher elevation. Most alpine lakes fall into this category. These pollen records typically offer a comprehensive overview of the regional high–altitude vegetation.
2. The pollen source area is also extensive, typically exceeding 30–50 km, but is devoid of surrounding mountains of higher elevation, such as the lower–altitude Menghai (MH) lake to the south (Tang, 1992). These records, similar to Type 1, encompass a diverse array of pollen sources and may also indicate vegetation changes across extensive regions. However, given the absence of high mountains in the surrounding area, the documented vegetation types are likely to resemble those in the vicinity of the sampling sites.
3. The pollen source area is limited, usually less than 10 km, yet surrounded by mountains of higher elevation, exemplified by the GC wetland (Deng et al., 2022). In this scenario, despite the presence of mountains surrounding the sedimentation site, the pollen assemblage is likely to be predominantly derived from local vegetation within the immediate area, owing to the limited capacity of the site to trap pollen grains.
4. The pollen source area is similarly limited (less than 10 km), without surrounding mountains of higher elevation, such as the NN wetland (this study). Pollen derived from this type of site predominantly reflects the composition of local vegetation, as there are no substantial topographic barriers that could interfere with pollen transport from distant sources. This characteristic renders it particularly valuable for investigating local–scale vegetation succession.

In summary, the first type of pollen records generally reflects regional high mountain vegetation, while the latter three types primarily represent local vegetation changes (Fig. 8).

Table 2
The basic information for pollen records in SW China.

Site	Long (°E)	Lan (°N)	Elevation (m a.s.l)	bottom Age (ka)	Sedimentary environment	Type	References
Tiancai (TC)	99.72	26.63	3898	21	Lake	1	Xiao et al., 2014a; Xiao et al., 2014b
Wuxu (WX)	101.40	29.15	3760	12.3	Lake	1	Zhang et al. (2016); Shen and Xiao (2018)
Shudu (SD)	99.94	27.91	3620	30	Lake	1	Cook et al. (2011); Cook et al. (2013); Yao et al., 2017
YSL profile	99.70	29.87	3310	32	Mountain	1	Shi et al. (2011)
Haligu (HLG)	100.18	27.00	3277	9.3	Lake	1	Song et al. (2012)
Wenhai (WH)	100.17	26.98	3080	23	Lake	1	Yao et al. (2015)
Lugu (LG)	100.78	27.72	2690	22	Lake	1	Shen and Xiao (2018)
Caohai (CH)	104.34	26.81	2203	22	Lake	1	Zhang et al. (2024)
Heqing (HQ)	100.17	26.56	2190	2780	Basin	1	Xiao et al. (2007); Jiang et al. (2001)
Niangniang (NN)	104.82	26.10	2000	37	Wetland	4	This study
Eryuanxihu (EYXH)	100.00	26.00	1980	17	Lake	1	Lin et al. (1986)
Erhai (EH)	100.18	25.73	1974	13	Lake	1	Shen et al. (2006)
Dianchi (DC)	102.68	25.02	1886	20	Lake	1	Xiao et al. (2020)
Tengchongqinghai (TCQH)	98.53	25.26	1885	68	Lake	1	Xiao et al. (2015); Yang et al. (2016); Zhang et al. (2020)
Ganchi (GC)	103.03	29.39	1805	25	Wetland	3	Deng et al. (2022)
Yangzonghai (YZH)	103.00	24.91	1800	13	Lake	1	Wang et al. (2020)
Xingyun (XY)	102.55	24.33	1717	37	Lake	1	Chen et al. (2014a); Chen et al. (2014b);
Chenghai (CHH)	100.67	26.53	1503	8.2	Lake	1	Xiao et al. (2017)
Yilong (YL)	102.58	23.68	1414	27	Lake	1	Li et al. (2024)
Dayin (DY)	105.04	24.23	991	47	Cave	4	Zhang et al. (2024)
Menghai (MH)	100.47	21.97	612	42	Lake	2	Tang, 1992

In numerous such records, from high–altitude regions in SW China and low–altitude areas on the southeastern margin of the Tibetan Plateau, it is evident that *Quercus* (ES) pollen was exceptionally abundant during the late MIS3 to the LGM. For instance, several lacustrine records, such as DC (Xiao et al., 2020), XY (Chen et al., 2014a), TCQH (Xiao et al., 2015; Zhang et al., 2020), and the HQ basin (Jiang et al., 2001), indicate the dominance of *Quercus* (ES) together with alpine *Abies/Picea* and cold–tolerant herbs in the vicinity of lakes in SW China. These pollen records, as described above, provide clear evidence that the ESQF expanded significantly southward and into lower-altitude regions during the period from MIS 3 to the LGM, in comparison to its modern distribution. Wang et al. (2023) utilized the MaxEnt model to simulate the potential distribution range of ESQF during the LGM, with results confirming this conclusion. However, it should be noted that all these pollen records belong to the Type 1 we previously classified (Table 2). Since these records may reflect surrounding mountain vegetation types rather than local vegetation changes, they might have overestimated the extent of ESQF expansion during the LGP. For instance, the pollen record from the relatively southern XY lake likely represents the mountain vegetation on its eastern side (1900–2500 m) (Chen et al., 2014a) (Fig. 8), while at an altitude of the core site (ca. 1700 m), it may be predominantly dominated by DBLF. This finding is also supported by records from the more southerly but lower–altitude YL lake (Li, K. et al., 2024). These examples demonstrate that failing to differentiate between regional (mountain–influenced) and local vegetation signals may result in misinterpretations regarding the actual extent of vegetation range shifts (Fig. 9a). In a recent study, three pollen records were utilized in the East Asian Monsoon Domain, comprising two from SW China (TCQH and CH) and one from central China (DJH), to quantitatively reconstruct the paleoclimate variations since the LGP (Zhang et al., 2023). The result shows that during the LGM, ESQF dominated around TCQH and CH lakes. Compared to modern vegetation, the altitudinal distribution of this vegetation zone shifted downward by ca. 900–1100 m (Zhang et al., 2020). Based on East Asian Pollen Database and quantitative models, it can be estimated that the MAT during the LGM was ca. 7–9 °C lower than during the Holocene (Zhang et al., 2023). However, given that the primary pollen sources of TCQH and CH predominantly originate from the surrounding alpine vegetation, it is plausible to infer that the ESQF did not extend to the same altitude around the two lakes during this period (Fig. 8). According to our NN records, the vegetation at ca. 2000 m likely represented either the lower boundary of the ESQF or the upper boundary of the DBLF. Consequently, the ESQF might have only undergone a vertical migration of 600–800 m during the LGM. Considering the slightly higher temperature gradient rate during the LGM compared to present–day conditions (Loomis et al., 2017), it is estimated that the MAT might have only decreased by an average of 5–7 °C relative to the Holocene. This finding is in good agreement with global model predictions (Osman et al., 2021), which not only validates the reliability of our estimations but also provides valuable insights into the regional climate changes during the LGM.

The deglaciation event since the LGM led to significant climatic changes, which in turn exerted profound impacts on the distribution and dynamics of vegetation types. As the climate gradually warmed and precipitation patterns altered, low–altitude vegetation types such as EBLF began to experience changes in their geographical ranges (Wang et al., 2019). Since the deglaciation, low–altitude vegetation types such as EBLF have restrictedly expanded northward (Zheng et al., 2023). However, the biome scores for DBLF recorded by NN, DC, and GC remained consistently high. Moreover, the proportion of deciduous components in southern sites, as documented by the studies of YZH (Wang et al., 2020), YL (Li, K. et al., 2024), and XY (Chen et al., 2014a), also remained relatively high. In contrast to the general northward expansion trend, the northward migration range of EBLF during this period was restricted, with its vertical distribution not exceeding 1400–1600 m a.s.l. This might be due to competition with other vegetation types, especially the persistent dominance of DBLF in some areas. Meanwhile, DBLF, ESQF and CLMX gradually migrated to higher–altitude areas in the eastern part of the Tibetan Plateau (Wang et al., 2019). For instance, the biome types in CH and TCQH underwent a clear transition from ESQF to DBLF, indicating that DBLF had vertically migrated to approximately 2000 m a.s.l. (Zhang et al., 2020, 2024). Nonetheless, records from HQ (Jiang et al., 2001), EYXH (Lin et al., 1986), and WH (Yao et al., 2015) still predominantly exhibit ESQF or CLMX, suggesting that DBLF in SW China was likely concentrated between 2000 and 2800 m a.s.l. during this period. Similarly, based on records from LG (Shen and Xiao., 2015), SD (Cook et al., 2011, 2013; Yao et al., 2017), WX (Zhang et al., 2016), TC (Xiao et al., 2014) and YSL (Shi et al., 2011), it can be inferred that ESQF in the area was distributed between 2400 and 3700 m a.s.l., while CLMX and ALSM were found at relatively higher altitudes (Fig. 9b).

With the gradual rise in temperature and precipitation, the EBLF, primarily consisting of *Castanopsis*, *Cyclobalanopsis*, and Euphorbiaceae,

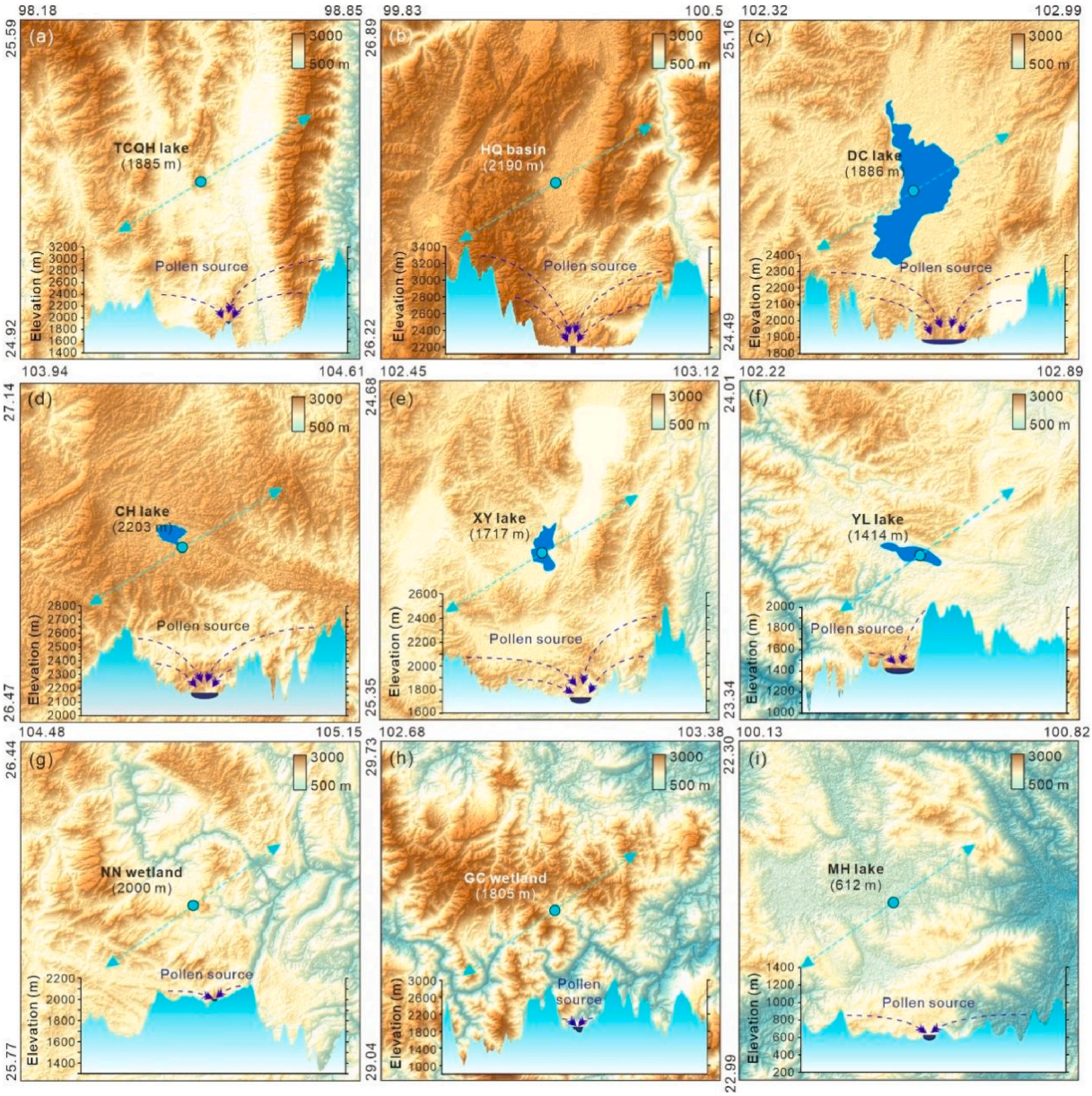

Fig. 8. The sedimentary environment and pollen sources documented by certain pollen records in SW China. (a) TCQH lake (Xiao et al., 2015; Zhang et al., 2020); (b) HQ basin (Jiang et al., 2001; Xiao et al., 2007); (c) DC lake (Xiao et al., 2020); (d) CH lake (Zhang et al., 2024); (e) XY lake (Chen et al., 2014a, 2014b); (f) YL lake (Li, K. et al., 2024); (g) NN wetland (this study); (h) GC wetland (Deng et al., 2022); (i) MH lake (Tang, 1992).

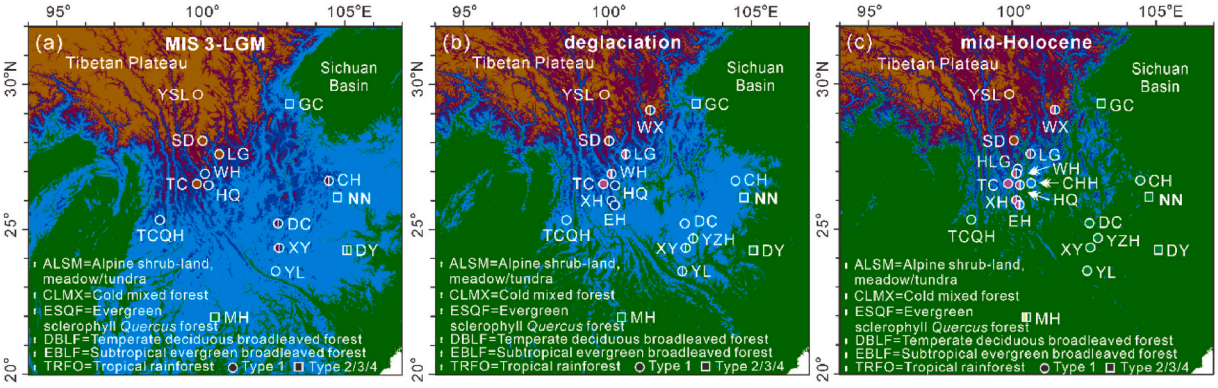

Fig. 9. Vegetation changes in Southwest China during (a) MIS3–LGM, (b) deglaciation and (c) early–mid Holocene inferred from pollen records and topographic feature.

experienced significant northward expansion during the early to mid-Holocene (Tang, 2015). This expansion and upward altitudinal shift not only demonstrated the vegetation's adaptability to climatic changes but also imposed ecological pressure on the distribution of DBLF, resulting in a marked contraction of its geographic range. Concurrently, paleovegetation records from high-altitude sites such as TCQH (Xiao et al., 2015; Zhang et al., 2020), CH (Zhang et al., 2024), GC (Deng et al., 2022), EH (Shen et al., 2006), and HQ (Jiang et al., 2001) reveal a transitional shift in vegetation composition, from DBLF dominance to an increased presence of evergreen elements. This suggests that the EBLF biome underwent a vertical shift to elevations of ca. 2200–2400 m a.s.l. (Fig. 9c). In contrast, the distribution range of DBLF was notably restricted. Based on records from WH (Yao et al., 2015), HLG (Song et al., 2012), LG (Xiao and Shen., 2018) and others, it can be inferred that the upper limit of DBLF distribution during this period was below approximately 3000 m a.s.l. A recent study by Zheng et al. (2023) examined the characteristics of EBLF and DBLF changes during the glacial to interglacial transition using pollen records from subtropical China. The findings revealed that most mountainous regions in the subtropical zone were predominantly covered by DBLF during the LGM, and the major biome replacement from deciduous to evergreen forest did not occur until around 8.1 ka. This suggests an earlier forest replacement in low–latitude regions compared to sites further north or at higher elevations. It not only provides additional evidence for the biome replacement process but also helps to establish a broader context for understanding the spatial and temporal patterns of vegetation changes in the region.

Following the LGP, the climate in the study region underwent significant changes, which had profound impacts on the distribution and migration of vegetation types. Among these, the ESQF, which exhibited a wide distribution during the LGP, gradually migrated to the southeastern edge of the Tibetan Plateau and the western margin of the Sichuan Basin. This migration resulted in its concentration primarily between 3000 and 3700 m a.s.l., similar to the modern distribution pattern (Yang et al., 2009). Meanwhile, pollen records from MH lake during the early–mid Holocene in southern regions highlighted specific components that are characteristic of TRFO (Tang, 1992). In contrast, NPK records from the Indochinese Peninsula at lower latitudes indicated that this region was predominantly covered by a typical TRFO biome during the same period (Penny, 2001). Consequently, it is reasonable to deduce that TRFO expanded from areas such as the Indochinese Peninsula into low–altitude regions south of ca. 22°N in SW China during this period. However, due to insufficient paleovegetation records, the precise extent of this expansion remains undetermined.

5.3. Possible climate forcing for the biome succession

Numerous studies have demonstrated that climate change since the LGP has significantly influenced biome succession across various regions in SW China (Xiao et al., 2020; Wang et al., 2019; Zhang et al., 2024). Understanding these impacts is essential for forecasting future ecosystem changes and for reconstructing the historical ecological dynamics of the region. For example, a continuous pollen record from 68 ka at TCQH lake indicates that vegetation during the MIS3 was highly productive (Zhang et al., 2020). By integrating this record with two additional sites (CH and DJH), the comprehensive dataset enabled the quantitative reconstruction of temperature and precipitation changes within the Asian monsoon domain since the MIS3 (Zhang et al., 2023). The pollen data from TCQH provided insights into the types and abundances of plants present, which were then correlated with known climate–vegetation relationships. The data from the other sites complemented this information, helping to fill in gaps and validate the reconstruction. These findings align with our PCA indicators for temperature (PC1) and precipitation (PC2), providing confirmation that the MIS3 period was characterized by significant climatic fluctuations, specifically cold and humid conditions (Fig. 10). On the

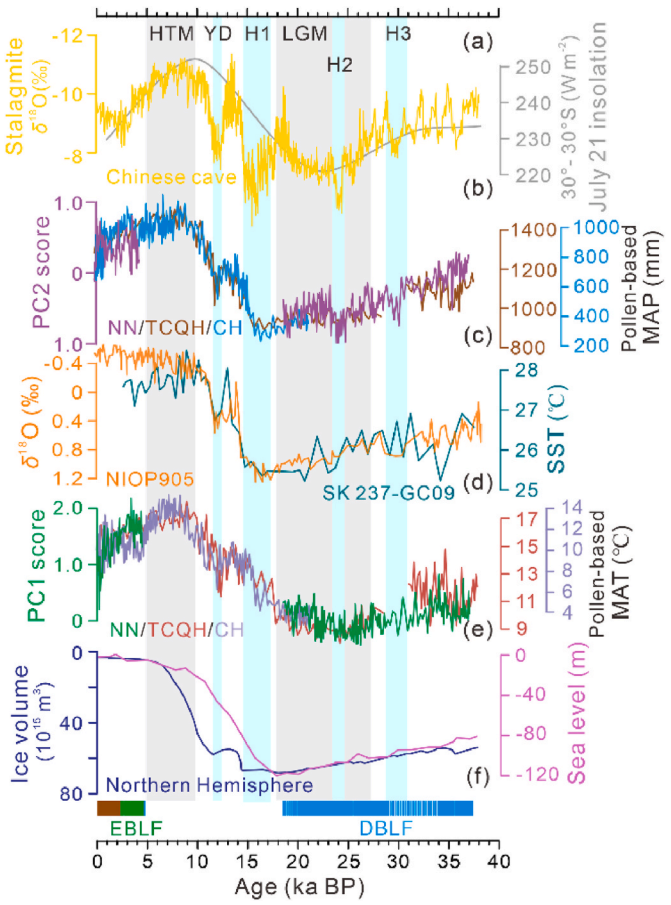

Fig. 10. Correlation of pollen proxies with other paleoclimatic records. (a) July 21 30°N–30°S insolation (Laskar et al., 2004) and Stalagmite $\delta^{18}O$ values from Chinese caves (Cheng et al., 2016); (b) PC2 for NN core and pollen–based MAP estimates for the TCQH and CH core (Zhang et al., 2023); (c) NIOP905 marine $\delta^{18}O$ *G. ruber* records (Jung et al., 2009) and SST from the SK237–GC09 core (Raza et al., 2017); (d) PC1 for NN core and pollen–based MAT estimates for the TCQH and CH core (Zhang et al., 2023); (e) ice volumes for the Northern Hemisphere simulated using ECHAM3 (Charbit et al., 2007) and sea level (Grant et al., 2014); (f) dominant biomes based on the NN core.

glacial–interglacial timescale, our PC1 and PC2 variations are closely correlated with Northern Hemisphere (NH) ice volume changes (Charbit et al., 2007) and the July insolation difference between 30°N and 30°S (Laskar et al., 2004), as shown in Fig. 10. This suggests that variations in ice sheets and the summer inter–tropical insolation gradient (SITIG) were critical factors influencing biome succession in SW China (Zhang et al., 2023, 2024). During the LGM, NH ice sheets significantly contributed to temperature reductions, intensifying the north–south temperature gradients. Consequently, this enhanced moisture transport from tropical oceans to the continent, increasing monsoonal precipitation over SW China and the eastern margin of the Tibetan Plateau (Lehmkuhl and Owen, 2005). The increased precipitation, in turn, influenced the growth and distribution of various plant taxa. Wet–adapted plants flourished, while drought–tolerant taxa encountered challenges, resulting in a shift in biome composition. Throughout this process, the Indo–Pacific Warm Pool played a crucial role in energy transmission, as evidenced by the high consistency between our pollen–based PC2 and other rainfall records in SW China (Xiao et al., 2020) with sea surface temperature (SST) and marine $\delta^{18}O$ data derived from planktonic foraminifera in the Bay of Bengal (Ahmad et al., 2012; Govil and Naidu, 2010; Jung et al., 2009).

Nonetheless, long–term climatic changes are insufficient to fully explain the intricate details of biome succession in SW China. For

instance, certain pollen records indicate that biomes underwent multiple distinct successions during deglaciation periods, frequently coinciding with rapid events such as the Younger Dryas (YD), Bolling–Allerød (BA), and H1 (Xiao et al., 2015; Zhang et al., 2024). Conversely, other pollen records suggest minimal or no significant changes in biome composition before and after these rapid events, with only a small fraction of species exhibiting minor alterations (Xiao et al., 2014; Shen and Xiao, 2018). This suggests that short–term fluctuations in regional climatic thresholds may have either facilitated or constrained the growth of certain taxa (Xu et al., 2023). Thus, the observed shifts in biomes in SW China are likely influenced by additional mechanisms rather than being solely a response to thermodynamic effects on a periodic scale. In this study, although YD and H1 are unrecorded, abrupt events H2 and H3 are distinctly evident in our precipitation indicators (PC2), indicating that the AMOC is an additional significant driver influencing changes in the Indian Monsoon, which profoundly affected the biome succession in SW China (Ng et al., 2018; Shen and Xiao, 2018). During the period of these abrupt events, the proportions of several taxa in our pollen records exhibited significant fluctuations. For example, Ericaceae, a taxon characterized by its representation as a typical deciduous shrub in subtropical regions (Tang, 2015), experienced a peak proportion of 11 % during the H2 event. In comparison with tree species such as *Quercus* (D), Ericaceae demonstrates a higher resilience to the strong winds and very dry conditions prevalent at mountain tops (Tang, 2015). Therefore, it is hypothesized that during the LGM, a period marked by an overall cold and dry climate, the exceptionally colder and drier conditions during the H2 event led to significant changes in certain taxa, such as Ericaceae. Similarly, biome transitions recorded by pollen analysis of CH lake since the LGM predominantly occurred during or immediately following global rapid events (i.e., H1, YD and the 4.2 ka event) (Zhang et al., 2024). Recently, the rainfall of the East Asian Summer Monsoon (EASM) was quantitatively reconstructed by using multi–proxy records from a maar lake in southern China, with the records dating back to the LGM (Lu et al., 2025). The analysis identified five critical tipping points in EASM rainfall variability since the LGM, which are also attributed to abrupt shifts in the AMOC and Saharan vegetation. Thus, the AMOC significantly impacts the degree of change in Asian monsoon precipitation through complex water vapor circulation processes, thereby influencing biome succession in SW China since the MIS3. These findings highlight the complex interplay between global climate systems, such as the AMOC, and regional ecological processes in the eastern margin of the Tibetan Plateau.

6. Conclusion

Studying the vegetation dynamics and biome variations in SW China is crucial for understanding the region's ecological history and its response to climate change. Our high–resolution pollen analysis yields a novel record of these aspects since 37 ka, enabling a detailed quantitative reconstruction of biome variations. The findings reveal that during the MIS3 period, the region surrounding the study site was dominated by DBLF, with *Quercus* (D) and other Betulaceae taxa serving as key components. The biome score for DBLF slightly decreased during the LGM, yet it remained the highest among all biomes. The discrepancies in biome composition during this period compared to records from the nearby CH lake may be attributed to variations in topographic characteristics and sedimentary environments. Through a comparative analysis of our findings with other pollen records from SW China, we infer that during the LGP, the DBLF likely expanded over extensive areas at medium to high altitudes in the region, whereas the ESQF may have experienced only a vertical migration of approximately 600–800 m during the LGM. Consequently, we hypothesize that the discrepancy in previous pollen-based MAT estimates may have been overestimated from the LGM to the Holocene.

In addition, during this period, the dominant vegetation type surrounding the NN wetland transitioned from DBLF to EBLF. This indicates that the EBLF biome in SW China underwent a vertical migration during the Holocene, establishing itself at elevations of approximately 2200–2400 m a.s.l. This shift not only indicates a response to changing climate conditions but also reflects the dynamic nature of the regional vegetation, adapting to gradual warming and other environmental factors. Over the past 2400 years, there has been a gradual shift towards the ALSM biome, with dominant taxa comprising pioneer plants and/or secondary shrubs associated with high fire frequencies. Consequently, we propose that this most recent biome transition is predominantly attributed to early human activities.

The PCA of the fossil pollen dataset revealed a strong correlation between the principal components and the simulated climate variables, indicating that PCA can serve as a robust proxy for assessing climate conditions. Given that abrupt events are clearly reflected in our precipitation indicators (PC2), we propose that, in addition to glacial–interglacial scale drivers such as solar radiation and variations in high–latitude ice volume, the AMOC plays an additional critical role in modulating changes in the Indian Monsoon. This, in turn, has significantly influenced biome transitions in SW China.

Author contributions

Xiao Zhang: Conceptualization, Data curation, Funding acquisition, Supervision, Writing–original draft, Writing–review & editing. Yuanfu Yue: Conceptualization, Data curation, Investigation, Formal analysis, Funding acquisition, Methodology, Supervision, Writing–review & editing. Ziyan Zhang: Software, Validation. Liuying He: Formal analysis, Writing–review & editing. Xinmeng Yuan: Formal analysis, Writing–review & editing. Xintian Yu: Formal analysis, Writing–review & editing. Qiuchi Wan: Investigation. Cong Chen: Investigation. Yongjie Tang: Investigation. Zhuo Zheng: Conceptualization, Methodology, Writing–review & editing. Kangyou Huang: Conceptualization, Writing–review & editing.

Declaration of competing interest

The authors declare that they have no known competing financial interests or personal relationships that could have appeared to influence the work reported in this paper.

Acknowledgments

This work was supported by the National Natural Science Foundation of China (41902184, 42366002 and 41702182) and National Key Research and Development Program of China (2022YFF0801501).

Data availability

A link to the data and/or code is provided as part of this submission.

References

Ahmad, S.M., Zheng, H.B., Raza, W., Zhou, B., Lone, M.A., Raza, T., Suseela, G., 2012. Glacial to Holocene changes in the surface and deep waters of the northeast Indian Ocean. Mar. Geol. 329, 6–23. https://doi.org/10.1016/j.margeo.2012.10.002.

Birks, H.J.B., Frey, D.G., Deevey, E.S., 1998. Review1: numerical tools in palaeolimnology progress, potentialities and problems. J. Paleolimnol. 20, 307–332. https://doi.org/10.1023/A:1008038808690.

Blaauw, M., Christen, J.A., 2011. Flexible paleoclimate age-depth models using an autoregressive gamma process. Bayesian Anal 6, 457–474. https://doi.org/10.1214/11-BA618.

Boufford, D.E., van Dijk, P.P., 2004. Mountains of Southwest China. In: Mittermeter, R. A., Gil, P.R., Hoffman, M., et al. (Eds.), Hotspot Revisited: Earth's Biologically Richest and Most Endangered Ecoregions. Cemex, Mexico, pp. 159–164, 2nd.

Braak, C.J.F.T., Smilauer, P., 2002. CANOCO Reference Manual and Cano-Draw for Windows User's Guide: Software for Canonical Community Ordination. Microcomputer Power, Ithaca, New York. Version 4. 5.

Charbit, S., Ritz, C., Philippon, G., Peyaud, V., Kageyama, M., 2007. Numerical reconstructions of the Northern Hemisphere ice sheets through the last glacial-interglacial cycle. Clim. Past. 3, 15–37. https://doi.org/10.5194/cp-3-15-2007.

Chen, F.H., Chen, X.M., Chen, J.H., Zhou, A.F., Wu, D., Tang, L.Y., Zhang, X.J., Huang, X. Z., Yu, J.Q., 2014b. Holocene vegetation history, precipitation changes and Indian Summer Monsoon evolution documented from sediments of Xingyun Lake, south-west China. J. Quat. Sci. 29, 661–674. https://doi.org/10.1002/jqs.2735.

Chen, X.M., Chen, F.H., Zhou, A.F., Huang, X.Z., Tang, L.Y., Wu, D., Zhang, X.J., Huang, X.Z., Yu, J.Q., 2014a. Vegetation history, climatic changes and Indian summer monsoon evolution during the Last Glaciation (36,400-13,400 cal yr BP) documented by sediments from Xingyun Lake, Yunnan, China. Paleogeogr. Paleoclimatol. Paleoecol. 410, 179–189. https://doi.org/10.1016/j.palaeo.2014.05.027.

Cheng, H., Edwards, R.L., Sinha, A., Spötl, C., Yi, L., Chen, S.T., Kelly, M., Kathayat, G., Wang, X.F., Li, X.L., Kong, X.G., Wang, Y.J., Ning, Y.F., Zhang, H.W., 2016. The Asian monsoon over the past 640,000 years and ice age terminations. Nature 534, 640–646. https://doi.org/10.1038/nature18591.

Chevalier, M., Davis, B.A.S., Heiri, O., Seppä, H., Chase, B.M., Gajewski, K., Lacourse, T., Telford, R.J., Finsinger, W., Guiot, J., Kühl, N., Maezumi, S.Y., Tipton, J.R., Carter, V.A., Brussel, T., Phelps, L.N., Dawson, A., Zanon, M., Vallé, F., Nolan, C., Mauri, A., Vernal, A., Izumi, K., Holmström, L., Marsicek, J., Goring, S., Sommer, P. S., Chaput, M., Kupriyanov, D., 2020. Pollen-based climate reconstruction techniques for late Quaternary studies. Earth Sci. Rev. 210, 103384. https://doi.org/10.1016/j.earscirev.2020.103384.

Cook, C.G., Jones, R.T., Langdon, P.G., Leng, M.J., Zhang, E.L., 2011. New insights on late Quaternary Asian palaeomonsoon variability and the timing of the Last Glacial Maximum in southwestern China. Quat. Sci. Rev. 30, 808–820. https://doi.org/10.1016/j.quascirev.2011.01.003.

Cook, C.G., Jones, R.T., Turney, C.S.M., 2013. Catchment instability and Asian summer monsoon variability during the early Holocene in southwestern China. Boreas 42 (1), 224–235. https://doi.org/10.1111/j.1502-3885.2012.00287.x.

Deng, Y.K., Ma, C.M., Huang, M., Zhao, L., Shang, G.C., Tang, L.Y., Lu, H.Y., 2022. Vegetation and climate changes since the Last Glacial Maximum inferred from high-resolution pollen records from the Sichuan Basin, southwest China. Palaeogeogr. Palaeoclimatol. Palaeoecol. 606, 111231. https://doi.org/10.1016/j.palaeo.2022.111231.

Flora of China Editorial Committee, 2013. Flora of China. Science Press, Beijing.

Govil, P., Naidu, P.D., 2010. Evaporation-precipitation changes in the eastern Arabian Sea for the last 68 ka: implications on monsoon variability. Paleoceanography 25, 1–19. https://doi.org/10.1029/2008PA001687.

Grant, K.M., Rohling, E.J., Ramsey, C.B., Cheng, H., Edwards, R.L., Florindo, F., Heslop, D., Marra, F., Roberts, A.P., Tamisiea, M.E., Williams, F., 2014. Sea-level variability over five glacial cycles. Nat. Commun. 5, 5076. https://doi.org/10.1038/ncomms6076.

Grimm, E.C., 1991. TILIA 2.0 (Computer Software) Illinois State. University Research and Collection Center.

Jiang, X.Z., Yang, X.D., Wang, S.M., Tong, G.B., 2001. The last glacial maximal pollen record in the lake sediments from ancient Heqing lake and its significance for paleomonsoon. Acta Micropalaeontol. Sin. 18, 263–267.

Jung, S.J.A., Kroon, D., Ganssen, G., Peeters, F., Ganeshram, R., 2009. Enhanced Arabian Sea intermediate water flow during glacial North Atlantic cold phases. Earth Planet Sci. Lett. 280, 220–228. https://doi.org/10.1016/j.epsl.2009.01.037.

Kong, F.C., Yang, R.D., Lin, S.J., 2010. Analysis of the evolution of Karst environment of Weining region, Guizhou Province west China: a proof from the sediment evolution of lake Caohai since about 73 million years. Earth Environ. 38, 138–145. https://doi.org/10.14050/i.cnki.1672-9250.2010.02.018.

Laskar, J., Robutel, P., Joutel, F., Gastineau, M., Correia, A.C.M., Levrard, B., 2004. A long term numerical solution for the insolation quantities of the Earth. Astron. Astro Phys. 428, 261–285. https://doi.org/10.1051/0004-6361:20041335.

Lehmkuhl, F., Owen, L.A., 2005. Late quaternary glaciation of tibet and the bordering mountains: a review. Boreas 34, 87–100. https://doi.org/10.1080/03009480510012908.

Li, K., Liao, M., Ni, J., 2024. Vegetation response to climate change and human activity in southwestern China since the last Glacial Maximum. Palaeogeogr. Palaeoclimatol. Palaeoecol. 636, 111990. https://doi.org/10.1016/j.palaeo.2023.111990.

Li, S.M., Wei, L.S., Zhao, W.W., Ren, W.H., Gu, Q.R., Che, Z.X., Cao, X.Y., Li, H., Zhang, X.J., Chen, C.Z., Zhao, Y., 2024. Environmental changes and human impacts over the past 1200 years: evidence from high-resolution pollen records from peat in the Yunnan-Guizhou Plateau, Southwest China. Palaeogeogr. Palaeoclimatol. Palaeoecol. 655, 112540. https://doi.org/10.1016/j.palaeo.2024.112540.

Li, Z., Saito, Y., Dang, P.X., Matsumoto, E., Vu, Q.L., 2009. Warfare Rather than Agriculture as a Critical Influence on Fires in the Late Holocene, Inferred from Northern Vietnam, vol 106. P.N.A.S, pp. 11490–11495. https://doi.org/10.1073/pnas.0813258106.

Lin, S.M., Qiao, Y.L., Walker, D., 1986. Late Pleistocene and Holocene vegetation history at Xi Hu, Er Yuan, Yunnan Province, southwest China. J. Biogeogr. 13, 419–440. https://doi.org/10.2307/2844966.

Liu, Z.Y., Otto-Bliesner, B.L., He, F., Brady, E.C., Tomas, R., Clark, P.U., Carlson, A.E., Lynch-Stieglitz, J., Curry, W., Brook, E., Erickson, D., Jacob, R., Kutzbach, J., Cheng, J., 2009. Transient simulation of last deglaciation with a new mechanism for Bølling-Allerød warming. Science 325, 310–314. https://doi.org/10.1126/science.1171041.

Loomis, S.E., Russell, J.M., Verschuren, D., Morrill, C., Cort, G.D., Damsté, J.S.S., Olago, D., Eggermont, H., Street-Perrott, F.A., Kelly, M.A., 2017. The tropical lapse rate steepened during the last glacial maximum. Sci. Adv. 3, e1600815. https://doi.org/10.1126/sciadv.1600815.

Lu, F.Z., Lu, H.Y., Gu, Y., Lin, P.Y., Lu, Z.Y., Zhang, Q., Zhang, H.Y., Yang, F., Dong, X.Y., Yi, S.W., Chen, D.L., Pausata, F.S.R., Ben-Yami, M., Mecking, J.V., 2025. Tipping point-induced abrupt shifts in east asian hydroclimate since the last glacial maximum. Nat. Commun. 16, 477. https://doi.org/10.1038/s41467-025-55888-w.

Moore, P.D., Webb, J.A., Collinson, M.E., 1991. Pollen analysis. J. Ecol. 80, 216.

Ng, H.C., Robinson, L.F., McManus, J.F., Mohamed, K.J., Jacobel, A.W., Ivanovic, R.F., Gregoire, L.J., Chen, T.Y., 2018. Coherent deglacial changes in western Atlantic Ocean circulation. Nat. Commun. 9, 1–10. https://doi.org/10.1038/s41467-018-05312-3.

Ni, J., Cao, X.Y., Jeltsch, F., Herzschuh, U., 2014. Biome distribution over the last 22,000 yr in China. Palaeogeogr. Palaeoclimatol. Palaeoecol. 409, 33–47. https://doi.org/10.1016/j.palaeo.2014.04.023.

Osman, M.B., Tierney, J.E., Zhu, J., Tardif, R., Hakim, G.J., King, J., Poulsen, C.J., 2021. Globally resolved surface temperatures since the last Glacial Maximum. Nature 599, 239–244. https://doi.org/10.1038/s41586-021-03984-4.

Pan, Z.K., Sun, Q.F., Wang, M., Meng, H.W., Huang, L.P., Shen, C.M., 2025. Dynamics of Yunnan pine (*Pinus yunnanensis*) forest since the Last Glacial Maximum in central Yunnan, SW China. Rev. Palaeobot. Palyno. 336, 105311. https://doi.org/10.1016/j.revpalbo.2025.105311.

Penny, D., 2001. A 40000 year palynological record from north-east Thailand; implications for biogeography and palaeo-environmental reconstruction. Paleogeogr. Paleoclimatol. Paleoecol. 171, 97–128. https://doi.org/10.1016/S0031-0182(01)00242-5.

Raza, T., Ahmad, S.M., Steinke, S., Raza, W., Lone, M.A., Beja, S.K., Suseela, G., 2017. Glacial to Holocene changes in sea surface temperature and seawater δ18O in the northern Indian Ocean. Paleogeogr. Paleoclimatol. Paleoecol. 485, 697–705. https://doi.org/10.1016/j.palaeo.2017.07.026.

Shen, J., Jones, R.T., Yang, X., Dearing, J.A., Wang, S., 2006. The holocene vegetation history of lake erhai, yunnan province southwestern China: the role of climate and human forcings. Holocene 16 (2), 265–276. https://doi.org/10.1191/0959683606hl923rp.

Shen, J., Xiao, X.Y., 2018. Evolution of the south Asian monsoon during the last 20 ka recorded in lacustrine sediments from southwestern China. Quat. Sci. 38, 799–820. https://doi.org/10.11928/j.issn.1001-7410.2018.04.01 (in Chinese).

Shi, S.Q., Yuan, D.X., Luo, L.D., Hao, X.D., Zhao, Z.Y., 2011. Comparative study on climatic change during later period of the late Pleistocene epoch with the sporopollen record from northwest Yunnan plateau and the stalagmite record from South China. Carsol. Sin./Zhong Guo Yan Rong 30 (2), 9. https://doi.org/10.3969/j.issn.1001-4810.2011.02.001 (in Chinese).

Song, X.Y., Yao, Y.F., Wortley, A.H., Paudayal, K.N., Blackmore, S., 2012. Holocene vegetation and climate history at haligu on the Jade Dragon Snow mountain, yunnan, sw China. Clim. Change 113 (3–4), 841–866. https://doi.org/10.1007/s10584-011-0364-6.

Tang, L.Y., 1992. Vegetation and climate history at Menghai, Yunnan during the past 42000 years. Acta Micropalaeontol. Sin. 9, 433–455 (in Chinese).

Tang, Q., 2015. The subtropical vegetation of Southwestern China. Plant Distribution, Diversity and Ecology. Springer, Netherlands. https://doi.org/10.1007/978-94-017-9741-2.

Wang, M., Meng, H.W., Huang, L.P., Sun, Q.F., Zhang, H.C., Shen, C.M., 2020. Vegetation succession and forest fires over the past 13000 years in the catchment of Yangzonghai Lake, Yunnan. Quaternary Science 40 (1), 175–189. https://doi.org/10.11928/j.issn.1001-7410.2020.01.17 (in Chinese).

Wang, W.M., Li, C.H., Shu, J.W., Chen, W., 2019. Changes of vegetation in southern China. Sci. China Earth Sci. 62, 1316–1328. https://doi.org/10.1007/s11430-018-9364-9.

Xiao, X.Y., Haberle, S.G., Shen, J., Yang, X.D., Han, Y., Zhang, E.L., Wang, S.M., 2014. Latest Pleistocene and Holocene vegetation and climate history inferred from an alpine lacustrine record, northwestern Yunnan Province, southwestern China. Quat. Sci. Rev. 86, 35–48. https://doi.org/10.1016/j.quascirev.2013.12.023.

Xiao, X.Y., Haberle, S.G., Li, Y.L., Liu, E.F., Shen, J., Zhang, E.L., Yin, J.J., Wang, S.M., 2017. Evidence of Holocene climatic change and human impact in northwestern Yunnan Province: High-resolution pollen and charcoal records from Chenghai Lake, southwestern China. Holocene 28, 127–139. https://doi.org/10.1177/0959683617715692.

Xiao, X.Y., Shen, J., Haberle, S.G., Han, Y., Xue, B., Zhang, E.L., Wang, S.M., Tong, G.B., 2015. Vegetation, fire, and climate history during the last 18500 cal a BP in southwestern Yunnan Province, China. J. Quat. Sci. 30, 859–869.

Xiao, X.Y., Shen, J., Wang, S.M., Xiao, H.F., Tong, G.B., 2007. Palynological evidence for vegetational and climatic changes from the HQ deep drilling core in Yunnan Province, China. Sci. China Earth Sci. 50, 1189–1201.

Xiao, X.Y., Yao, A., Hillman, A., Shen, J., Haberle, S.G., 2020. Province based on high-resolution pollen and charcoal records from Dianchi, southwestern China. Quat. Sci. Rev. 236, 106297. https://doi.org/10.1016/j.quascirev.2020.106297.

Xu, D.K., Lu, H.Y., Chu, G.Q., Shen, C.M., Sun, Q., Wu, J., Li, F.J., Song, B., Cui, A.N., Li, H., Wu, N.Q., 2023. Fast response of vegetation in East Asia to abrupt climatic events during the last deglaciation. In: Proc. Natl. Acad. Sci. U.S.A. Nexus, 2, pp. 1–10. https://doi.org/10.1093/pnasnexus/pgad061.

Xu, Q.H., Zhang, S.R., Gaillard, M., Li, M.Y., Cao, X.Y., Tian, F., Li, F.R., 2016. Studies of modern pollen assemblages for pollen dispersal- deposition- preservation process understanding and for pollen-based reconstructions of past vegetation, climate, and human impact: a review based on case studies in China. Quaternary Sci. Rev. The International Multidisciplinary Review Journal 149.

Yang, Q.S., Chen, W.Y., Xia, K., Zhou, Z.K., 2009. Climatic envelope of evergreen sclerophyll oaks and their present distribution in the eastern Himalaya and Hengduan Mountains. J. Systemat. Evol. 47, 183–190. https://doi.org/10.1111/j.1759-6831.2009.00020.x.

Yang, Y.P., Zhang, H.C., Chang, F.Q., Meng, H.W., Pan, A.D., Zheng, Z., Xiang, R., 2016. Vegetation and climate history inferred from a Qinghai Crater Lake pollen record

from Tengchong, southwestern China. Paleogeogr. Paleoclimatol. Paleoecol. 461, 1–11. https://doi.org/10.1016/j.palaeo.2016.07.017.
Yao, Y.F., Song, X.Y., Wortley, A.H., Wang, Y.F., Blackmore, S., Li, C.S., 2017. Pollen-based reconstruction of vegetational and climatic change over the past ~30 ka at Shudu Lake in the Hengduan Mountains of Yunnan, southwestern China. PLoS One 12 (2), e0171967. https://doi.org/10.1371/journal.pone.0171967.
Yao, Y.F., Song, X.Y., Wortley, A.H., Blackmore, S., Li, C.S., 2015. A 22 570-year record of vegetational and climatic change from wenhai lake in the hengduan mountains biodiversity hotspot, yunnan, southwest China. Biogeosciences 12 (5), 1525–1535. https://doi.org/10.5194/bg-12-1525-2015.
Yue, Y., Zheng, Z., Huang, K., Chevalier, M., Chase, B.M., Carré, M., Ledru, M.P., Cheddadi, R., 2012. A continuous record of vegetation and climate change over the past 50,000 years in the Fujian Province of eastern subtropical China. Palaeogeogr. Palaeoclimatol. Palaeoecol. 365–366, 115–123. https://doi.org/10.1016/j.palaeo.2012.09.018.
Yue, Y.F., He, L.Y., Zheng, Z., Chen, C., Wan, Q.C., Tang, Y.J., Huang, K.Y., 2024. Late Holocene vegetation succession, climate change, and fire history in western Guizhou. Quaternary Science 44, 112–127. https://doi.org/10.11928/i.issn.1001-7410.2024.01.09 (in Chinese).
Zeng, H., Wang, Z.Y., Chen, G.X., Ferguson, D.K., Wang, Y.F., Yao, Y.F., 2025. Asian summer monsoon and orographic winds change the pollen flow in the Hengduan Mountains, southwestern China. Geophys. Res. Lett. 52, e2024GL113697. https://doi.org/10.1029/2024GL113697.
Zhang, E., Wang, Y., Sun, W., Shen, J., 2016. Holocene Asian monsoon evolution revealed by a pollen record from an alpine lake on the southeastern margin of the Qinghai–Tibetan Plateau. China, Clim. Past 12, 415–427. https://doi.org/10.5194/cp-12-415-2016.
Zhang, J.X., Xu, H., Gosling, W.D., Lan, J.H., Dodson, J., Lu, F.Y., Yu, K.K., Sheng, E.G., Liu, B., 2019. Vegetation and climate evolution during the Last Glaciation at Tengchong in Yunnan Province, Southwest China. Paleogeogr. Paleoclimatol. Paleoecol. 514, 441–452. https://doi.org/10.1016/j.palaeo.2018.11.008.
Zhang, X.S., 2007. Vegetation Map of the People's Republic of China (1:1 000 000). Geology Press, Beijing.
Zhang, X., Huang, K.Y., Zheng, Z., Zhang, Y.Z., Wan, Q.C., Tian, L.P., 2018. Pollen morphology of Quercus sect. Ilex and its relevance for fossil pollen identification in southwest China. Grana 57, 401–414. https://doi.org/10.1080/00173134.2018.1480653.
Zhang, X., Zheng, Z., Huang, K.Y., Cheng, J., Cheddadi, R., Zhao, Y., Chen Liang, C., Yang, X.Q., Wan, Q.C., Tang, Y.J., Chen, C., Li, J., 2023. Quantification of Asian monsoon variability from 68 ka BP through pollen-based climate reconstruction. Sci. Bull. 68, 713–722. https://doi.org/10.1016/j.scib.2023.03.013.
Zhang, X., Zheng, Z., Huang, K.Y., Yang, X.Q., Tian, L.P., 2020. Sensitivity of altitudinal vegetation in southwest China to changes in the Indian summer monsoon during the past 68000 years. Quat. Sci. Rev. 239, 106359. https://doi.org/10.1016/j.quascirev.2020.106359.
Zhang, Y., Yang, Q., Yang, F., Zeng, Y.M., Zhang, Z.T., Yang, W.S., Zou, Z.N., Shi, L., Zheng, H.B., 2024. Environment evolution and human activities since MIS3 at Dayindong site, Yunnan. Quaternary Sci. 44 (1), 29–47. https://doi/10.11928/j.issn.1001-7410.2024.01.03 (in Chinese).
Zhao, Y., Yu, Z.C., Herzschuh, U., Yang, B., Zhao, H., Fang, K.Y., Li, H., Li, Q., 2014. Vegetation and climate change during Marine Isotope Stage 3 in China. Chin. Sci. Bull. 59, 4444–4455. https://doi.org/10.1007/s11434-014-0611-0.
Zheng, Z., Chen, C., Huang, K.Y., Zhang, X., Kershaw, P., Cheng, J., Li, J., Yue, Y.F., Wan, Q.C., Zhang, Y.Z., Tang, Y.J., Wang, M.Y., Xiao, X.Y., Cheddadi, R., 2023. Holocene warming and evergreen/deciduous forest replacement across eastern China. Quat. Sci. Rev. 307, 108057. https://doi.org/10.1016/j.quascirev.2023.108057.
Zheng, Z., Zhang, X., Man, M.L., Wei, J.H., Huang, K.Y., 2016. Review and data integration of pollen-based quantitative Paleoclimate reconstruction studies in China and adjacent areas. Quat. Sci. 36, 503–519 (in Chinese).
Zhou, G.Y., 1981. Discussion on the boundary of warm temperature deciduous broad-leaf forest region in China. Acta Phytoecologia et Geo botanica Sinica 5. https://doi.org/10.1021/ol3026507 (in Chinese).
Zhou, X.P., Tang, L.Y., Xia, H.X., Peng, T., Deng, X.Y., Hou, M.D., Zhu, D., Xie, R.L., Wang, B., Guo, Y., 2022. Bryoflora characteristics in Niangniang Mountain national wetland Park. Liupanshui. Guizhou. J. Trop. Subtrop. Bot. 30, 111–124 (in Chinese).
Zhou, Z.K., Yang, Q.S., Xia, K., 2007. Fossils of *Quercus* sect. *Heterobalanus* can help explain the uplift of the Himalayas. Chin. Sci. Bull. 52, 238–247. https://doi.org/10.1007/s11434-007-0005-7.